Received: 21 June 2022 | Revised: 5 August 2022 | Accepted: 13 August 2022

DOI: 10.1002/aic.17880

AIChE JOURNAL

RESEARCH ARTICLE

Reaction Engineering, Kinetics and Catalysis

Taylor-vortex membrane reactor for continuous gas–liquid reactions

Baldassarre Venezia[1] | David C. Morris[2] | Asterios Gavriilidis[1]

[1]Department of Chemical Engineering, University College London, London, UK

[2]Autichem Ltd, Warrington, Cheshire, UK

Correspondence
Asterios Gavriilidis, Department of Chemical Engineering, University College London, Torrington Place, London WC1E 7JE, UK.
Email: a.gavriilidis@ucl.ac.uk

Funding information
Engineering and Physical Sciences Research Council, Grant/Award Number: EP/L003279/1

Abstract

A unique Taylor-vortex membrane reactor (TVMR) design for continuous gas–liquid reactions is presented in this work. The reactor consists of a cylindrical rotor inside a stationary concentric cylindrical vessel, and a flexible system of equispaced baffle rings surrounding the rotor. This restricts the annular cross section to a small gap between the baffles and the rotor, and divides the annulus into 18 mixing zones. The baffles support a 6 m long PFA tubular membrane that is woven around the rotor. At 4 mL/min inlet flow rate, the TVMR showed a plug-flow behavior and outperformed the unbaffled reactor, having 5–12 times lower axial dispersion. The continuous aerobic oxidation of benzyl alcohol was performed for 7 h using the $Pd(OAc)_2$/pyridine catalyst in toluene at 100 °C and 1.1 MPa oxygen pressure. A stable conversion of 30% was achieved with 85% benzaldehyde selectivity, and no pervaporation of organics into the gas phase.

KEYWORDS
Taylor–Couette reactor, membrane reactor, axial dispersion, catalytic aerobic oxidation, process intensification

1 | INTRODUCTION

Multiphase reactions are omnipresent in industry and reactor design plays an important role in managing interphase mixing, reactant mass transfer, heat transfer and residence time distribution.[1,2] Continuous flow reactors can provide enhanced control over mixing, improved thermal management and safer access to hazardous chemistries with respect to conventional batch reactors.[3] However, flow patterns and transport phenomena vary as a function of the scale, and need to be thoroughly assessed in order to preserve process safety and product quality.[4–6]

Taylor-vortex reactors are characterized by having high mass and heat transfer coefficients and can minimize macroscopic backmixing, while intensifying mixing at the smaller scales (meso and micromixing).[7] A Taylor-vortex system generally consists of a cylindrical rotor inside a stationary concentric cylindrical vessel. The fluid in the annulus undergoes different fluid dynamic regimes depending on the rotor speed, as well as the geometry and the configuration of the annulus between the rotor and the vessel.[8–10] At low rotor angular speeds, the fluid in the annulus of a Taylor-vortex system is characterized by a *laminar Couette flow*, which is a purely azimuthal laminar flow around the rotor. However, above a critical value of the rotor angular speed, and depending on the annulus aspect ratio and inner-to-outer annulus radius ratio, the hydrodynamic instability of the centrifugal flow generates laminar counter-rotating toroidal vortices around the rotor, stacked on one another. This regime is characterized by a low intervortex (macromixing) and high intravortex mixing (mesomixing) and is widely known as *Taylor-vortex flow*. Taylor vortices can be beneficial in reaction engineering, as they can enlarge the contact surface area between reacting phases and narrow the residence time distribution, by approaching the behavior of CSTRs in series. These features have

made the Taylor-vortex reactor popular across different scales and applications such as in polymerizations,[11,12] electrochemistry,[13–15] biochemistry,[16,17] crystallization,[18] graphene production,[19,20] and in photo-,[21–23] homogeneous[24] and heterogeneous catalysis.[22,23]

Taylor-vortex devices have also been used in gas–liquid applications, such as in the crystallization of calcium carbonate,[25–28] algal growth by bubbling carbon dioxide in the annulus[29,30] and in photo-oxidations using molecular oxygen.[31,32] Studies on the flow patterns,[33–35] and on mixing and mass transfer[30,36–40] of gas bubbles inside the Taylor-vortex annulus demonstrated that the gas–liquid mass transport is a complex function of the bubble size and spatial distribution, the azimuthal Reynolds number and the horizontal or vertical orientation of the device. To ensure that gas delivery is disconnected from the liquid fluid dynamics in the annulus, membranes can be adopted. The use of membranes in flow reactors have gained popularity owing to their ability to provide control of exothermic gas–liquid reactions, by distributing and dosing gaseous reactants while physically separating the two reacting phases.[41–44]

Wroński *et al.* demonstrated a Taylor-vortex membrane device that consisted of a cylindrical rotor inside a stationary tubular ceramic membrane.[45] Gas was pressurized outside the membrane and, depending on its pressure with respect to the liquid, diffusion or bubbling could be achieved. Other works report the use of a membrane as a rotor in a Taylor-vortex device for various applications such as blood component separation,[46–50] reverse osmosis,[51–54] and filtration of emulsions,[55,56] suspensions[57–60] and proteins.[61] In all these studies, the high-speed rotating filter membrane created an intense shear rate, which, together with the effect from the Taylor vortices, reduced concentration polarization and increased filtration rate.[51,52] However, both the inner-rotating and the outer-static membrane designs offer a surface area for gas delivery that is fixed and strictly dependent on the reactor configuration. Furthermore, in certain applications, for example, gas–liquid aerobic oxidations, the use of dense gas-permeable membranes that can easily be sealed and connected to the gas line, are desirable to avoid breakthrough of gas into the liquid.

In this work, the first example of a Taylor-vortex reactor with a tubular membrane inside the reactor annulus, for continuous gas–liquid reactions is demonstrated. The reactor consists of a cylindrical rotor inside a stationary concentric cylindrical vessel, with a tubular membrane wound in the annulus around the rotor and supported by a flexible and replaceable system of baffles, that almost completely fill the annular gap and divide the annulus into 18 axially-segregated compartments.

2 | MATERIALS AND METHODS

2.1 | Reactor design

The Taylor-vortex membrane reactor (TVMR) is based on a cylindrical rotor that rotates around its axis inside a concentric cylindrical vessel

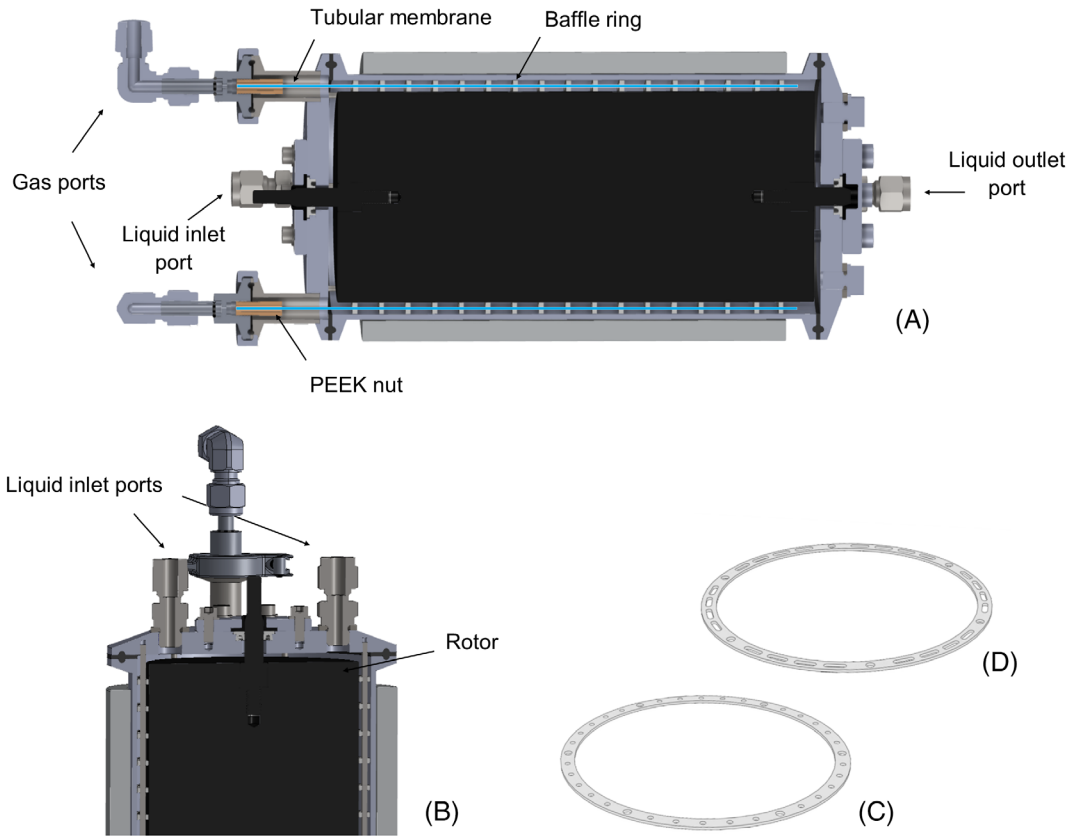

FIGURE 1 (A) Axial section of the Taylor-vortex membrane reactor. (B) Inlet side of the reactor with sections of the liquid inlet ports. (C) PTFE baffle rings with circular holes and (D) slots, that can be used to support the tubular membrane in the Taylor-vortex membrane reactor

(see Figure 1). The vessel has an internal diameter of 97.6 mm, a length of 202 mm, and is sealed on two flanges using a 4″ high-pressure tri-clamp (Advanced Couplings Limited) and a PTFE envelope gasket for each side. Inside the vessel, a 196 mm long carbon-filled poly ether ketone (PEEK) cylindrical rotor with a diameter of 87.6 mm is fitted in the inlet flange via a Kefloy rotary seal (MupuSeal). This creates an annulus with the stationary vessel that has a rotor-to-inner vessel radius ratio, η, of 0.898 and an aspect ratio, Γ, of 40, defined as the ratio between the vessel length and the annulus gap. The inlet flange has four ports, two of which are designed for the gas inlet and outlet. The gas ports are 33.5 mm long with an inner diameter of 9.5 mm, and a PEEK 1/4–28 UNF nut is hosted in each port to seal the tubular membrane (see Figure 1A). These nuts are screwed inside two outer clamp ferrules, that host the gas for reaction and that are sealed to the two gas ports using 1/2″ high pressure tri-clamps (Advanced Couplings Limited) and PTFE envelope gaskets. The other two ports on the inlet flange are 1/4″ Swagelok connections and are used for introducing the liquid reactants (Figure 1B). Similarly and symmetrically to the inlet flange, the outlet side of the reactor has two ports for the liquid outlet.

Surrounding the rotor, six equispaced stainless steel threaded studs (M2.5 × 196 mm) are screwed on the liquid side of the inlet flange. They support a system of 17 baffles that divide the annulus into 18 axially-segregated sections. The baffles are rings made of PTFE with a thickness of 1.3 mm, and an inner and outer diameter of 88.6 and 97.5 mm. These dimensions allow them to span the whole annular cross section, leaving a gap of approximately 0.5 mm from the rotor. Each baffle is separated by a 10 mm gap using stainless steel hollow cylinder spacers (2.5 mm ID, 3 mm OD, 10 mm long), inserted into each threaded stud and between adjacent baffles. Table 1 summarizes the characteristic dimensions of the Taylor-vortex membrane reactor.

To demonstrate the use of a membrane in a gas–liquid reaction, a 6 m long polyfluoro alkoxy (PFA, 1/16″ OD × 0.040″ ID, Idex) tube was inserted inside the structure of baffles around the rotor. The type of baffle used to support the PFA membrane is shown in Figure 1C. This has 36 equidistributed holes, 6 with a diameter of 2.7 mm and the remaining 30 with a 1.5 mm wide hole. The threaded studs were inserted in the larger holes, while the tubular membrane was woven through the smaller ones inside the annulus and around the rotor.

PFA has been successfully used in a previous study as a tubular membrane for oxygen delivery in gas–liquid aerobic oxidation of alcohols.[62] For this reason and for ease of installation, the PFA tubular membrane was selected to be tested in the TVMR. The reactor also offers the possibility to install any flexible tubular membrane by using baffles with different hole sizes and shapes, including slots for less flexible membranes (see Figure 1D). To seal the membrane, the two sides of the PFA tube were connected to the two PEEK 1/4–28 UNF nuts in each gas port (Figure 1A). The tri-clamps were then used to complete the sealing. Figure 2 shows a picture of the reactor with and without the outer vessel, and the PFA tubular membrane inserted through the baffles along the axial direction, bending in U-shapes at each end of the baffle system. Once the membrane spanned the whole azimuthal coordinate around the rotor, it was connected to the outlet gas port.

TABLE 1 Taylor-vortex membrane reactor dimensions

Property	Value
Rotor radius (r_i), mm	43.8
Vessel inner radius (r_o), mm	48.8
Baffle inner radius ($r_{b,i}$), mm	44.3
Baffle outer radius ($r_{b,o}$), mm	48.8
Radius ratio (η), –	0.898
Vessel length (L), mm	202
Interbaffle distance (h_b), mm	10
Vessel annulus aspect ratio (Γ), –	40
Interbaffle annulus aspect ratio (Γ_b), –	2

2.2 | Setup description and operation

The schematic of the setup is shown in Figure 3, and a picture of the equipment is reported in the Supplementary Material. The rotor was connected via a flexible coupling to a drive (Masterflex L/S 7524–55, Cole Parmer) with adjustable speed. The substrate and catalyst solutions were delivered separately using high pressure dual piston pumps

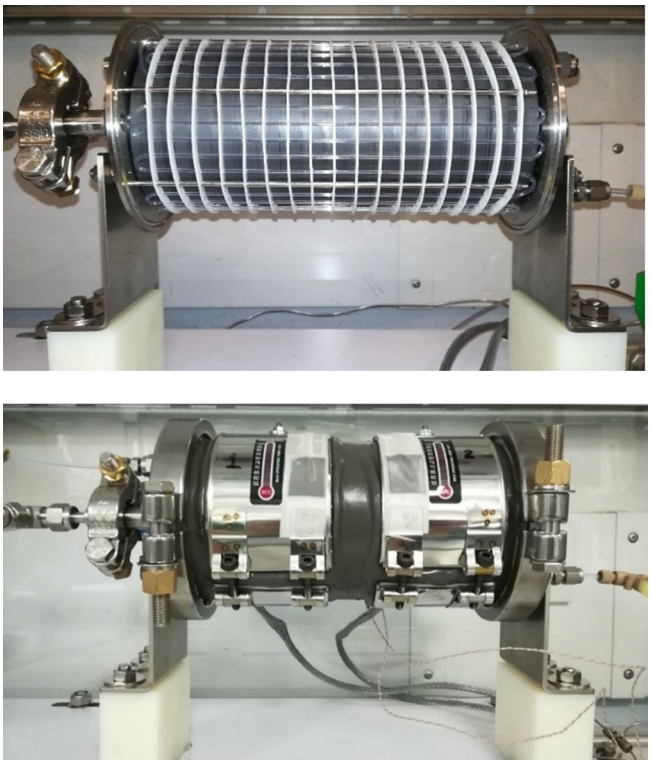

FIGURE 2 Taylor-vortex membrane reactor without the outer vessel showing the tubular membrane around the rotor (top), and with the outer vessel and the two external heaters (bottom)

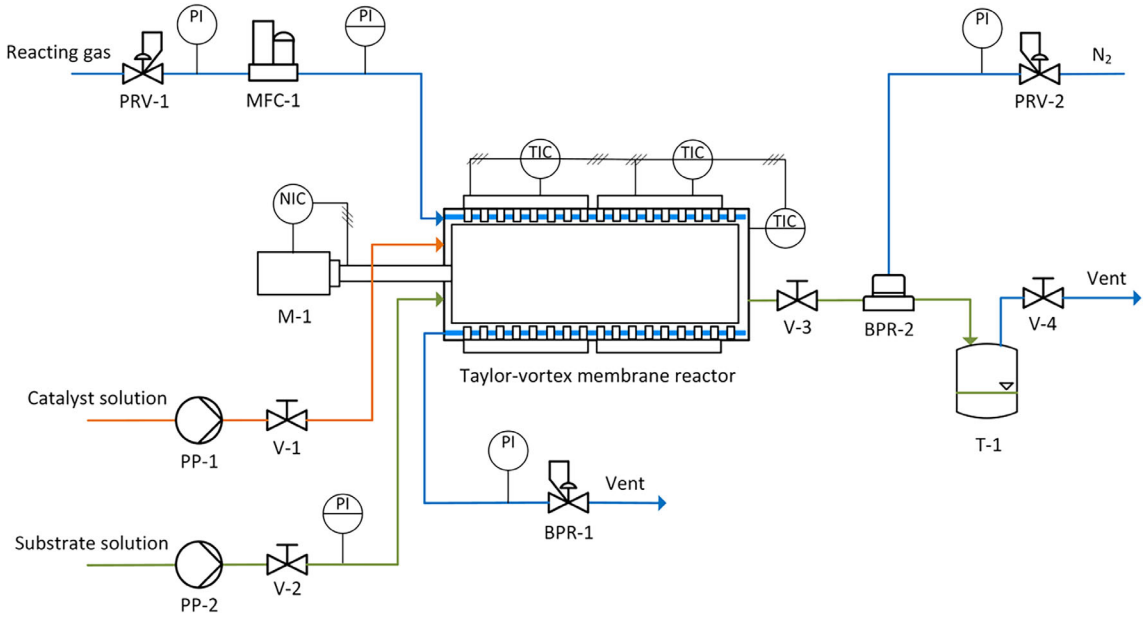

FIGURE 3 Schematic diagram of the Taylor-vortex membrane reactor setup. BPR: back-pressure regulator, M: drive, MFC: mass flow controller, NIC: angular speed indicator-controller, PI: pressure indicator, PP: piston pump, PRV: pressure reducing valve, T: collection vessel, TIC: temperature indicator-controller, V: shut-off valve.

for the catalyst (Azura P2.1S Knauer) and for the substrate solution (Vapourtec R2 pump). The pumps were connected to the two liquid inlet ports on the reactor flange. On the outlet flange, one of the two liquid outlet ports was connected to a back-pressure regulator (BPR, Zaiput), while the second one was used for inserting a process thermocouple (T type, RS Components). The BPR maintained the desired liquid pressure upstream using a gas pressure regulator (KPR, Swagelok) on the nitrogen line connected to the BPR. Liquid products were collected in a 250 mL glass vessel (Schott), which was occasionally emptied to avoid overfilling. The liquid pressure was constantly monitored using a pressure sensor (PX309, Omega) connected to the substrate inlet line, which was kept 0.1 MPa higher than the gas pressure, to avoid breakthrough of the gas into the organic solution inside the reactor. Gas was fed into the membrane inlet port after reducing its pressure with a gas pressure regulator (KPR, Swagelok) and adjusting its flow rate with a mass flow controller (4850, Brooks). The gas outlet port on the reactor inlet flange was connected to a gas back-pressure regulator (KBP, Swagelok) to maintain a constant gas pressure upstream.

High temperature was attained using two Mica band heaters (500 W, Elmatic) that surrounded the outer vessel of the reactor. Their power was controlled by a supervisory control box to which the process thermocouple was connected. As the two heaters could reach a maximum temperature of 300 °C, two additional thermocouples were embedded under the two heaters to measure their temperature and allow control of their output power. Along with the target process temperature, the supervisory box required to specify the maximum differential temperature between the jacket, measured by the two heater thermocouples, and the process temperature, measured by the process thermocouple. This avoided exposing the reactor to excessively high wall temperatures. Between the Mica band heaters and the reactor vessel a 2 mm silicone thermal interface pad (4.5 W/m/K, RS components) was used to fill the gap and increase heat transfer to the reactor walls. Furthermore, to provide external insulation, a 6.35 mm thick silicone sponge sheet (Silex Silicones) was wrapped around the reactor.

2.3 | Macromixing study

Macromixing was evaluated by studying the residence time distribution (RTD) of a tracer in the Taylor-vortex membrane reactor. Experiments were conducted by performing a pulse-input injection of the tracer (Basic Blue 3, Sigma Aldrich) in the reactor filled with deionized water, at atmospheric pressure and room temperature (21 °C). A volume of 3 mL of the tracer at a concentration of 7.5 g/L in deionized water was filled in a PFA capillary tube (1/16″ OD × 0.040″ ID, Idex). This was connected to the liquid inlet port of the reactor and to a milliGAT LF pump (VICI Valco) that supplied water at a constant flow rate. The Taylor-vortex membrane reactor was run at an agitation speed of 1.0–8.4 rad/s and the RTD was studied at a pump flow rate of 4 and 6 mL/min. Furthermore, for comparison and to understand the effect of the baffles and the membrane on mixing, the RTD was studied in the reactor with neither the baffles nor the membrane in place, at a flow rate of 4 mL/min.

The tracer concentration was monitored at the reactor outlet using ultraviolet–visible (UV–vis) spectroscopy. The UV–vis flowcell was directly installed at the outlet of the reactor, and via optical fibers to a light source (DH-2000-BAL, Ocean Optics). The light beam was shone through the flow cell containing the outlet tube and transmitted to a spectrophotometer (USB2000+ UV–VIS-ES,

Ocean Optics). The DI water background was subtracted before the experiment and the intensity of the transmitted light was averaged between 645 and 660 nm, which corresponds to the wavelength range of the blue dye UV–vis absorption peak. The integration time was set to 30 ms and scans were taken approximately every 6 s for the experiments at 6 mL/min inlet flow rate, and 12 s for those at 4 mL/min. Data analysis was performed using the software Ocean Optics Spectra Suite.

A calibration of the spectrophotometer was carried out to ensure that the tracer outlet concentration lay within the range of linear response with the UV–vis absorbance. As a consequence, the residence time distribution, $E(t)$, was derived according to Equation (1), where $A(t)$ is the UV–vis absorbance. The mean residence time, τ, and the variance, σ^2, were determined by integrating the first and the second moment of $E(t)$, respectively, as shown in Equations (2) and (3). Using the closed–closed vessel boundary conditions, and assuming a perfect pulse at the liquid inlet, the dispersion number, D_{ax}/uL, which describes the extent of axial mixing, can be calculated by solving Equation (4), which is valid for large deviations from plug-flow ($D_{ax}/uL > 0.01$).[63] The dispersion number is a dimensionless number defined as the ratio between the dispersion coefficient, D_{ax}, and the product between u, the average axial velocity, and L, the distance between the inlet and the outlet.

$$E(t) = \frac{A(t)}{\int_0^\infty A(t)dt}, \tag{1}$$

$$\tau = \int_0^\infty t\,E(t)dt, \tag{2}$$

$$\sigma^2 = \int_0^\infty (t-\tau)^2\,E(t)dt, \tag{3}$$

$$\frac{\sigma^2}{\tau^2} = 2\left(\frac{D_{ax}}{uL}\right) - 2\left(\frac{D_{ax}}{uL}\right)^2\left(1 - e^{-\frac{uL}{D_{ax}}}\right). \tag{4}$$

In order to describe the fluid dynamic regime occurring in the Taylor-vortex system, dimensionless numbers can be used. The Taylor number, Ta, defined in Equation (5) describes the ratio between the governing rotational inertial forces and the viscous forces.[64] In this equation, Ω is the rotational speed (rad/s), r_i the rotor radius, r_o the internal radius of the vessel and ν the kinematic viscosity of the fluid. The ratio between the axial inertial forces and the viscous forces is characterized by the axial Reynolds number, Re, defined in Equation (6).

$$Ta = \frac{\Omega r_i(r_o - r_i)}{\nu}, \tag{5}$$

$$Re = \frac{u(r_o - r_i)}{\nu}. \tag{6}$$

The Schmidt number is also reported in this study, allowing the comparison of macromixing between reactors, where different liquids were used. This number is defined in Equation (7), where the molecular diffusivity of the tracer in water, D_m, is approximately 6.4×10^{-10} m^2/s,[65] and the kinematic viscosity of water, ν, is 10^{-6} m^2/s.

$$Sc = \frac{\nu}{D_m}. \tag{7}$$

2.4 | Continuous aerobic oxidation

The reactor was tested by performing the aerobic oxidation of benzyl alcohol using the $Pd(OAc)_2$ homogeneous catalyst with pyridine.[66–68] As elucidated in the work of Steinhoff *et al.*, this base is responsible for the stabilization and prevention of Pd^0 aggregation, which is generated from the reduction of $Pd(OAc)_2$, as the alcohol is oxidized to aldehyde.[67] Furthermore, pyridine is responsible for the increased reaction rate of Pd^0 with O_2, which re-oxidizes Pd back to its acetate form.

The reaction was conducted in toluene at 100 °C and 1.1 MPa oxygen pressure for 7 h, 2 h of which were required for start-up and 1 h for shut-down. Prior to the reaction, the reactor was placed vertically and loaded with a toluene solution of 0.15 mol/L benzyl alcohol (99.8%, Sigma-Aldrich) and 0.1 mol/L mesitylene (98%, Sigma-Aldrich), used as internal standard. After connecting the reactor to the gas and liquid lines, the drive was switched on and the angular speed was set to 3.1 rad/s. Two solutions were pumped into the reactor, one containing the substrate and the other the homogeneous catalyst solution. The substrate solution was made of 0.3 mol/L benzyl alcohol, 0.12 mol/L pyridine (>99.5%, Alfa Aesar) and 0.1 mol/L mesitylene, dissolved in toluene (HPLC grade, Fisher Scientific). The second solution was made of 0.03 mol/L $Pd(OAc)_2$ (47.5% Pd, ACROS Organics) and 0.1 mol/L mesitylene in toluene. The two solutions were each pumped at 2 mL/min, generating a total flow rate of 4 mL/min. The Zaiput back-pressure regulator was set to 1.2 MPa, while oxygen (N5.5, BOC) was fed at a constant flow rate of 30 NmL/min and at a pressure of 1.1 MPa into the

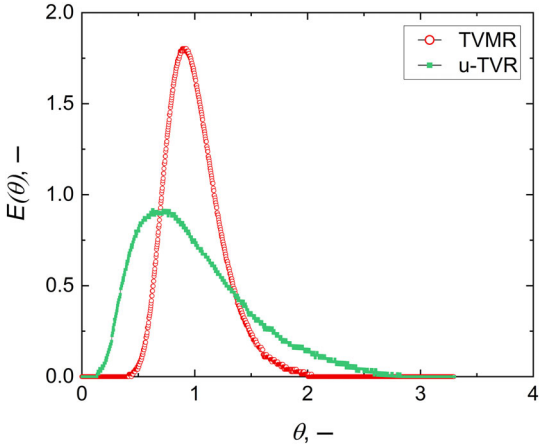

FIGURE 4 Residence time distribution, $E(\theta)$, in the Taylor-vortex membrane reactor (TMVR) and in the unbaffled Taylor-vortex reactor (u-TVR). Inlet flow rate: 4 mL/min ($Re = 0.23$), rotor angular speed: 1.0 rad/s ($Ta = 229$)

6 m long PFA tubular membrane (1/16″ OD × 0.040″ ID, Idex). The gas back-pressure regulator was venting the outlet oxygen gas into a GC vial immersed in an ice bath, in order to condense any volatile organics pervaporating through the membrane during reaction. The heaters were switched on and the process temperature setpoint was set to 100 °C, with a maximum temperature difference of 40 °C between the heaters and the process temperature. Gas chromatography (7820A, Agilent Technologies) was used to analyze the liquid products, with an automatic liquid sampler, a HP-INNOWAX (19091-133) capillary column and a flame ionization detector.

3 | RESULTS AND DISCUSSION

3.1 | Macromixing study

The residence time distribution of the tracer in the TVMR was characterized at different angular speeds and compared to that of the unbaffled Taylor-vortex reactor (u-TVR) at 4 mL/min inlet flow rate. Figure 4 shows two examples of normalized RTDs, $E(\theta)$, one for the TVMR and the other for the u-TVR, plotted against the normalized residence time, θ, both defined in Equation (8).

$$E(\theta) = \tau E(t);\ \ \theta = t/\tau. \tag{8}$$

For each inlet flow rate, the residence time in the TVMR was determined for different agitation speeds and averaged (*e.g.*, 71 min at 4 mL/min), and a liquid volume of approx. 280 mL was estimated. On the other hand, the tracer in the u-TVR had an average residence time of 83 min at 4 mL/min, which corresponded to a volume occupied by the liquid of *ca.* 330 mL. This is 50 mL higher than the TVMR, due to the absence of the baffles and the membrane. The average residence times resulting from this RTD study varied by ±6.1% across the various agitation speeds.

Figure 5 shows the dispersion number of the TVMR and the u-TVR for a range of Taylor numbers and axial Reynolds numbers. For reference, the dispersion numbers of 10 and 20 CSTRs in series are shown. The equivalent number of CSTRs in series, N, can be correlated to the dimensionless variance, σ^2/τ^2, using Equation (9).[63]

$$\frac{\sigma^2}{\tau^2} = \frac{1}{N}. \tag{9}$$

For comparison, the results from Richter *et al.* of the axial dispersion number obtained under a similar Re as in this work, are also reported in Figure 5.[64] In their work, the authors demonstrated how a modified rotor, segmented by horizontal ribs, inside a Taylor-vortex system could narrow the liquid residence time distribution by immobilizing the toroidal vortices and increasing vortex segregation, compared to a cylindrical rotor.

Concerning the unbaffled Taylor-vortex system (u-TVR) at $Re = 0.23$, the dispersion number increased from 0.140 ($N = 4.2$) to 0.609 ($N = 1.6$) for a Taylor number increasing from 229 to 1835. As

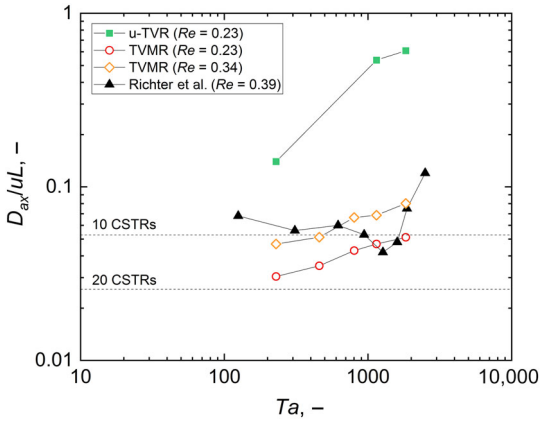

FIGURE 5 Dispersion number, D_{ax}/uL, in the unbaffled Taylor-vortex reactor (u-TVR) and in the Taylor-vortex membrane reactor (TMVR) at $Sc = 1563$. The dispersion numbers for 10 CSTRs and 20 CSTRs in series are shown for reference, along with results from the ribbed rotor Taylor-vortex reactor by Richter *et al.* ($Sc = 3276$)[64]

mentioned in the introduction, mixing in a Taylor-vortex reactor is closely bound to the fluid dynamic regime in the annulus.[69,70] Recktenwald *et al.* derived the critical Taylor numbers, Ta_c, above which the first flow instability between a laminar Couette and a laminar Taylor-vortex flow occurs.[71] The Ta_c is a function of the axial Reynolds number and the radius ratio, η. Given a $\eta = 0.898$ and $Re = 0.23$, for the u-TVR the $Ta_c = 130$, corresponding to a rotor speed of 0.6 rad/s. At increasing agitation speeds of the rotor, the flow regime transitions from a *laminar Taylor vortex flow* (TVF) to a time-dependent *wavy vortex flow* (WVF) with stacked Taylor vortices becoming azimuthal waves. At even higher rotor speeds, the flow becomes a *modulated wavy vortex flow* (MWVF) and finally, *turbulent* with multiple distinct turbulent regimes.[10,70,72,73] However, for high η the MWVF may not occur.[74] Nevertheless, while increasing the rotor speed, the degree of mixing grows at all scales until full backmixing is achieved. Using the fluid dynamic intervals reported by Nemri *et al.* for $\eta = 0.85$, the u-TVR would experience a WVF regime for $172 < Ta < 707$.[70] However, for Ta values up to 1192 the flow regime would lie within the MWVF, while above this value the flow would be turbulent. Therefore, it is reasonable to assume that the dispersion numbers for the u-TVR were obtained in three different flow regimes: a wavy vortex flow regime at $Ta = 229$ ($D_{ax}/uL = 0.134$), a modulated wavy vortex flow regime at $Ta = 1147$ ($D_{ax}/uL = 0.537$) and a turbulent Taylor-vortex flow at a $Ta = 1835$ ($D_{ax}/uL = 0.609$).

Concerning the TVMR, axial dispersion increased almost linearly in a log–log plot at increasing angular speeds for both axial flow rates. For a $Re = 0.23$ (4 mL/min), the dispersion number increased from 0.030 ($N = 16.9$) at $Ta = 229$ (1.0 rad/s) to 0.051 ($N = 10.3$) at $Ta = 1835$ (8.4 rad/s), and this range of axial dispersion is one order of magnitude lower than that achieved by the unbaffled reactor (u-TVR). Furthermore, it is interesting to observe that the highest equivalent number of CSTRs realized by the TVMR was 17 (16.9) at

1.0 rad/s, which is close to the number of interbaffle sections (18) that axially divide the reactor.

These differences can be ascribed to the different annulus configuration of the u-TVR and the TVMR. In fact, while the u-TVR has a cylindrical annulus with an aspect ratio of 40, the TVMR can be seen as made of a series of 18 Taylor-vortex units, each with an aspect ratio of 2, separated via baffle rings and intersected by 6 support rods and 30 times by the tubular membrane.

Inside an annulus with a small aspect ratio, the effect of the annulus boundaries becomes non-negligible and the flow pattern that develops differs from the axisymmetric spiraling motion previously mentioned in the introduction.[75] Multiple vortices can be present in a small annulus and their number and configuration depend on the rotor speed trajectory. Benjamin reported the fluid pattern inside an annulus with varying heights and with a constant annulus gap between a rotating cylinder and a stationary wall.[76,77] The author identified a primary Taylor-vortex flow that develops by a gradual increase in the Taylor number, featuring an even number of Taylor vortices when Ta is sufficiently high. However, other multiple steady and time-independent flow patterns, termed secondary modes, are formed when the rotor is suddenly accelerated from rest to above a certain value and disappear when Ta is reduced below this threshold. These secondary modes can be classified as normal or anomalous. The former are characterized by the presence of an even number of vortices, while the latter can either have an odd or an even number of Taylor vortices with at least one cell rotating outward near the annulus stationary boundary, contrary to what occurs in the primary mode.[75,78] Benjamin and Mullin mapped the anomalous modes for different Taylor numbers and aspect ratios ranging from 1.70 to 5.42 and they identified between 2 and 7 anomalous cells in the annulus. The authors used a 50 wt% glycerol mixture in water in an annulus with $\eta = 0.615$. For $\Gamma = 2.18$, a stable anomalous three-vortex mode was found at $Ta > 300$.[75] However, when decreasing the Taylor number below this value, the 3-cell abnormal mode collapsed into a normal spiraling two-vortex mode.[75]

Nakamura *et al.* also reported the anomalous 3-cell mode in a symmetrically closed annulus with $\eta = 0.669$ for $2.21 < \Gamma < 4.98$. At a lower aspect ratio, the flow bifurcates to either the normal 2-cell or the 4-cell mode.[78,79] For aspect ratios just below 2, a single anomalous vortex was also observed. This can occur in the presence of other smaller vortices. In particular, at $Ta = 566$ inside an annulus with $\Gamma = 1.71$ and $\eta = 0.669$, a one-cell vortex was observed coexisting with two smaller vortices at the corner between the upper plate and the outer cylinder (outer vortex) and between the upper plate and the rotor (inner vortex). However, as the aspect ratio approached 2 from 1, the inner smaller vortex became larger, merged with the outer vortex and the flow pattern bifurcated into a mode with two normal spiraling vortices.[79]

The presence of multiple vortices in each annular section of the TVMR may be responsible for the enhanced mesomixing that is observed, with respect to the u-TVR. Furthermore, the tubular membrane and the support rods that cross the interbaffle zones can cause disruption of the azimuthal flow, creating wake azimuthal vortices that can further enhance mesomixing.

The local mixing intensity alone cannot explain the axial dispersion difference between the TVMR and the unbaffled reactor. Mixing in a Taylor-vortex reactor under a continuous axial flow has been the subject of many works.[69,80–85] Axial dispersion in the unbaffled Taylor-vortex reactor is a function of inter- and intravortex mass transport phenomena,[85] as well as the convective transport across the vortex boundaries due to the axial flow rate.[69] Furthermore, under moderate axial flow rates, toroidal vortices move downstream, with the vortex shape and drift velocity being a function of the superficial axial velocity and the rotational speed.[71,86,87] On the other hand, the 0.5 mm gap between the rotor and the baffle rings in the TVMR represents the only cross sectional area in the 5 mm wide annulus gap for mass transport between the interbaffle zones. Moreover, the baffle rings physically hinder the downstream drifting of the vortices, decreasing axial dispersion with respect to the unbaffled reactor.

For $Re = 0.34$, corresponding to a flow rate of 6 mL/min, the dispersion number in the TVMR increased linearly from 0.047 ($N = 11.2$) at $Ta = 229$ to 0.080 ($N = 6.7$) at $Ta = 1835$, deviating from the equivalent number of 10 CSTRs in series for $Ta > 459$ (see Figure 5). While Moore and Cooney predicted a -0.83 exponent for the Re for the calculation of D_{ax}/uL,[69] axial dispersion in the TVMR increased as Re increased from 0.23 to 0.34. In particular, as Re increased 1.48 times from 0.23 to 0.34, the dispersion number increased on average by 1.52 for the various Taylor numbers. This almost linear dependency of the dispersion number on the axial flow rate is also found in laminar liquid flows with high Schmidt numbers,[63] suggesting that axial dispersion in the TVMR may be ascribed to the convective mass transport occurring in the gap region between the baffles and the rotor where the flow regime is laminar.

Vortex immobilization and a positive correlation between Re and D_{ax}/uL were also observed by Richter *et al.* in their Taylor-vortex reactor with a ribbed rotor.[64] The authors investigated the flow patterns in the gap between the rotor and the vessel at increasing Taylor numbers, and they discovered that the ribs around the rotor promoted vortex segregation and shifted the onset of turbulence to higher rotor speeds compared to the unribbed reactor. However, unlike in this study, axial dispersion in the Taylor-vortex reactor of Richter *et al.* did not show a monotonic increase for the explored range of Taylor numbers, but at $600 < Ta < 1800$ a minimum in the dispersion number was observed (see Figure 5), corresponding to $D_{ax}/uL = 0.042$ ($N = 12.4$). This occurred at the transition between the laminar Couette flow and the turbulent vortex flow ($Ta > 1200$) in the gap created between the rib and the vessel.

However, at $Ta > 1270$, the referenced reactor showed a steep increase in the dispersion number which exceeded 0.05 for $Ta > 1600$ and reached 0.12 at $Ta = 2500$. Under these conditions, a fully turbulent vortex flow regime characterized the fluid gap between the rotor and the vessel, which increased backmixing. On the other hand, the TVMR was able to maintain a lower dispersion number for $Ta < 620$ and a lower rate of increase of the dispersion number for $Ta > 1270$ than that of the ribbed Taylor-vortex reactor. This could be attributed

to the absence of a significantly wide gap between the stationary baffles and the rotor in the TVMR, which might have hindered the turbulent transition that Richter *et al.* observed between the rotating baffles and the outer stationary wall.

3.2 | Continuous aerobic oxidation reaction

The oxidation of benzyl alcohol was performed in the TVMR and results are shown in Figure 6. The reaction proceeded with 30% benzyl alcohol conversion and 85% selectivity to benzaldehyde, corresponding to a production of 5 g of benzaldehyde after 7 h of continuous operation. Steady-state in conversion and product selectivity was reached after 3 h from the start of the experiment, which is reasonable considering that the residence time was 70 min and the process temperature took some time to stabilize.

Ye *et al.* used the same $Pd(OAc)_2$/pyridine catalyst system in toluene for the aerobic oxidation of various alcohols.[68] Reactions were carried out in flow in a stainless-steel tube which could have an external jacket or be placed in a convection oven for temperature control. The catalyst solution containing 0.03 mol/L $Pd(OAc)_2$ was pre-mixed with 8% O_2/N_2 and then mixed with the substrate solution of 0.6 mol/L alcohol and 0.12 mol/L pyridine in toluene. Benzyl alcohol was oxidized at 100 °C and 500 psig (3.4 MPa) using an equal flow rate of 0.9 mmol/min for benzyl alcohol, the palladium catalyst and the oxygen gas, and a residence time of 2.5 h. The use of diluted oxygen ensured a safe operation outside the flammability region, and a yield of 87% to benzaldehyde was achieved, equivalent to 0.41 g/min of benzaldehyde produced per 1 g/min of flowing $Pd(OAc)_2$. At the end of the oxidation reaction, an amount of 8 g of benzaldehyde was isolated.

In contrast, the TVMR operated with a shorter liquid residence time (*ca.* 70 min) and with a substrate and catalyst flow rate of 2 mL/min. This corresponded to an inlet flow rate of 0.6 mmol/min of benzyl alcohol and 0.06 mmol/min of palladium, reacting to produce 1.26 g/min of benzaldehyde per 1 g/min of $Pd(OAc)_2$ catalyst. Furthermore, the use of a membrane controlled the mass transfer of oxygen from the gas phase to the palladium catalyst in the bulk liquid. After 7 h operation, fouling by palladium metal was observed in the inlet section of the reactor, which might have been caused by the incomplete re-oxidation of the palladium catalyst, possibly due to the excess of benzyl alcohol as compared to oxygen.[68] Nevertheless, the TVMR achieved a stable conversion and selectivity for 7 h under safe conditions due to the presence of a membrane that physically separated the oxidant from the organic phase. During reaction, no condensed organics were detected in the vial at the gas outlet, indicating that the reaction was conducted safely without the risk of forming a flammable gas mixture. This could be ascribed to the PFA membrane hindering the pervaporation of the organics from the hot liquid in the reactor to the gas phase.

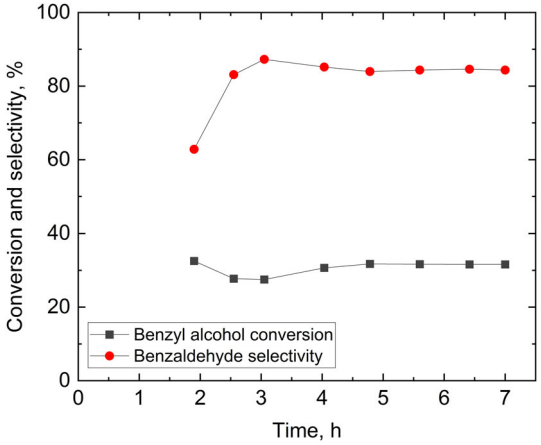

FIGURE 6 Benzyl alcohol conversion and benzaldehyde selectivity. Substrate solution: 0.3 mol/L benzyl alcohol, 0.12 mol/L pyridine and 0.1 mol/L mesitylene at 2 mL/min. Catalyst solution: 0.03 mol/L $Pd(OAc)_2$ and 0.1 mol/L mesitylene at 2 mL/min. Solvent: toluene, temperature: 100 °C, oxygen pressure: 1.1 MPa

4 | SUMMARY AND CONCLUSIONS

The Taylor-vortex membrane reactor (TVMR) is a continuous reactor that combines the mixing benefits deriving from toroidal Taylor vortices segregated by baffles in the annulus of a Taylor-vortex system, and the presence of a gas permeable tubular membrane for gas–liquid reactions. The reactor was manufactured using off-the-shelf, industrially tried and tested components, with only the rotor and baffles being bespoke designs. For this reason, the TVMR benefits from established and cost effective manufacturing methods and offers a viable route to larger scale. Residence time distributions showed a plug-flow behavior for an inlet flow rate of 4 mL/min and with rotor speeds ranging between 1.0 and 8.4 rad/s ($Ta = 229–1835$). Under these conditions, the equivalent number of CSTRs in series ranged from a maximum of 17 ($Ta = 229$) to 10 ($Ta = 1835$). However, when using 6 mL/min inlet flow rate, the equivalent number of CSTRs in series dropped below 10 for $Ta > 459$. Nevertheless, the TVMR outperformed the same reactor but without the baffles and membrane, showing a 4–6 times higher number of equivalent CSTRs in series. It also showed improved axial dispersion compared to a reported Taylor-vortex reactor with ribs on the rotor for $Ta > 1140$. This was possible owing to the baffle rings that supported the membrane and divided the annulus into segregated annular compartments. To demonstrate the application of this reactor to continuous gas–liquid reactions, the aerobic oxidation of benzyl alcohol was performed using the $Pd(OAc)_2$/pyridine catalyst system in toluene at 1.1 MPa oxygen pressure and 100 °C. Conversion and selectivity remained constant at 30% and 85% respectively, and 5 g benzaldehyde was produced after 7 h continuous operation. Furthermore, the risks associated with oxygen reacting with the organic substrate at a high temperature were overcome by using a perfluoro alkoxy membrane that separated the gas from the liquid phase.

NOMENCLATURE

Latin letters

A	UV–vis absorption, a.u.
D_{ax}	axial dispersion coefficient, m^2/s
D_m	molecular diffusivity, m^2/s
E	residence time distribution
h_b	interbaffle distance, mm
L	reactor vessel length, mm
N	number of CSTRs in series, –
Re	Reynolds number, –
$r_{b,i}$	baffle inner radius, mm
$r_{b,o}$	baffle outer radius, mm
r_i	rotor radius, mm
r_o	vessel inner radius, mm
Sc	Schmidt number, –
t	time, s
Ta	Taylor number, –
u	average velocity, m/s

Greek letters

Γ	vessel annulus aspect ratio $(r_o\text{-}r_i)/L$, –
Γ_b	interbaffle annulus aspect ratio $(r_o\text{-}r_i)/h_b$, –
η	radius ratio r_i/r_o, –
θ	dimensionless time, –
ν	kinematic viscosity, m^2/s
σ	standard deviation of the residence time distribution, s
τ	average residence time, s
Ω	rotor angular speed, rad/s

AUTHOR CONTRIBUTIONS

Baldassarre Venezia: Conceptualization (lead); data curation (lead); formal analysis (lead); investigation (lead); methodology (lead); visualization (lead); writing – original draft (lead); writing – review and editing (equal). **David C. Morris:** Conceptualization (supporting); resources (supporting); supervision (supporting); visualization (equal); writing – review and editing (equal). **Asterios Gavriilidis:** Funding acquisition (lead); methodology (supporting); project administration (lead); resources (lead); supervision (lead); writing – review and editing (equal).

ACKNOWLEDGMENTS

We thank EPSRC for funding (grant EP/L003279/1) and for BV's DTP studentship.

DATA AVAILABILITY STATEMENT

The data that support the findings of this study are available in the supplementary material of this article.

ORCID

Baldassarre Venezia https://orcid.org/0000-0002-3290-0420
Asterios Gavriilidis https://orcid.org/0000-0003-3508-5043

REFERENCES

1. Mills PL, Chaudhari RV. Multiphase catalytic reactor engineering and design for pharmaceuticals and fine chemicals. *Catal Today*. 1997;37:367-404.
2. Mills PL, Ramachandran PA, Chaudhari RV. Multiphase reaction engineering for fine chemicals and pharmaceuticals. *Rev Chem Eng*. 1992;8:1-176.
3. Wiles C, Watts P. Continuous flow reactors: a perspective. *Green Chem*. 2012;14:38-54.
4. Donati G, Paludetto R. Scale up of chemical reactors. *Catal Today*. 1997;34:483-533.
5. Kockmann N, Gottsponer M, Roberge DM. Scale-up concept of single-channel microreactors from process development to industrial production. *Chem Eng J*. 2011;167:718-726.
6. Nagy KD, Shen B, Jamison TF, Jensen KF. Mixing and dispersion in small-scale flow systems. *Org Process Res Dev*. 2012;16:976-981.
7. Schrimpf M, Esteban J, Warmeling H, Färber T, Behr A, Vorholt AJ. Taylor–Couette reactor: principles, design, and applications. *AIChE J*. 2021;67:e17228.
8. Coles D. Transition in circular Couette flow. *J Fluid Mech*. 1965;21:385-425.
9. Snyder HA. Waveforms in rotating Couette flow. *Int J Non Linear Mech*. 1970;5:659-685.
10. Andereck CD, Liu SS, Swinney HL. Flow regimes in a circular Couette system with independently rotating cylinders. *J Fluid Mech*. 1986;164:155-183.
11. Imamura T, Saito K, Ishikura S, Nomura M. A new approach to continuous emulsion polymerization. *Polym Int*. 1993;30:203-206.
12. Wei X, Takahashi H, Sato S, Nomura M. Continuous emulsion polymerization of styrene in a single Couette–Taylor vortex flow reactor. *J Appl Polym Sci*. 2001;80:1931-1942.
13. Rivero EP, Granados P, Rivera FF, Cruz M, González I. Mass transfer modeling and simulation at a rotating cylinder electrode (RCE) reactor under turbulent flow for copper recovery. *Chem Eng Sci*. 2010;65:3042-3049.
14. Coeuret F, Legrand J. Mass transfer at the electrodes of concentric cylindrical reactors combining axial flow and rotation of the inner cylinder. *Electrochim Acta*. 1981;26:865-872.
15. Love A, Lee DS, Gennari G, et al. A continuous-flow electrochemical Taylor vortex reactor: a laboratory-scale high-throughput flow reactor with enhanced mixing for scalable electrosynthesis. *Org Process Res Dev*. 2021;25:1619-1627.
16. Hill EK, Krebs B, Goodall DG, Howlett GJ, Dunstan DE. Shear flow induces amyloid fibril formation. *Biomacromolecules*. 2006;7:10-13.
17. Ameer GA, Harmon W, Sasisekharan R, Langer R. Investigation of a whole blood fluidized bed Taylor–Couette flow device for enzymatic heparin neutralization. *Biotechnol Bioeng*. 1999;62:602-608.
18. Barresi AA, Marchisio D, Baldi G. On the role of micro- and mesomixing in a continuous Couette-type precipitator. *Chem Eng Sci*. 1999;54:2339-2349.
19. Tran TS, Park SJ, Yoo SS, Lee T-R, Kim T. High shear-induced exfoliation of graphite into high quality graphene by Taylor–Couette flow. *RSC Adv*. 2016;6:12003-12008.
20. Nam K-H, Jung Kim U, Hee Jeon M, et al. Green, fast, and scalable production of reduced graphene oxide via Taylor vortex flow. *Chem Eng J*. 2019;391:123482.
21. Sengupta TK, Kabir MF, Ray AK. A Taylor vortex photocatalytic reactor for water purification. *Ind Eng Chem Res*. 2001;40:5268-5281.
22. Dutta PK, Ray AK. Experimental investigation of Taylor vortex photocatalytic reactor for water purification. *Chem Eng Sci*. 2004;59:5249-5259.
23. Sczechowski JG, Koval CA, Noble RD. A Taylor vortex reactor for heterogeneous photocatalysis. *Chem Eng Sci*. 1995;50:3163-3173.

24. Färber T, Riechert O, Zeiner T, Sadowski G, Behr A, Vorholt AJ. Homogeneously catalyzed hydroamination in a Taylor–Couette reactor using a thermomorphic multicomponent solvent system. *Chem Eng Res Des*. 2016;112:263-273.
25. Jung WM, Kang SH, Kim W-S, Choi CK. Particle morphology of calcium carbonate precipitated by gas–liquid reaction in a Couette–Taylor reactor. *Chem Eng Sci*. 2000;55:733-747.
26. Kang SH, Lee SG, Jung WM, et al. Effect of Taylor vortices on calcium carbonate crystallization by gas–liquid reaction. *J Cryst Growth*. 2003; 254:196-205.
27. Jung W-M, Hoon Kang S, Kim K-S, Kim W-S, Kyun CC. Precipitation of calcium carbonate particles by gas–liquid reaction: morphology and size distribution of particles in Couette–Taylor and stirred tank reactors. *J Cryst Growth*. 2010;312:3331-3339.
28. Kim W-S. Application of Taylor vortex to crystallization. *J Chem Eng Jpn*. 2014;47:115-123.
29. Kong B, Shanks JV, Vigil RD. Enhanced algal growth rate in a Taylor vortex reactor. *Biotechnol Bioeng*. 2013;110:2140-2149.
30. Gao X, Kong B, Vigil RD. Characteristic time scales of mixing, mass transfer and biomass growth in a Taylor vortex algal photobioreactor. *Bioresour Technol*. 2015;198:283-291.
31. Lee DS, Amara Z, Clark CA, et al. Continuous photo-oxidation in a vortex reactor: efficient operations using air drawn from the laboratory. *Org Process Res Dev*. 2017;21:1042-1050.
32. Lee DS, Sharabi M, Jefferson-Loveday R, Pickering SJ, Poliakoff M, George MW. Scalable continuous vortex reactor for gram to kilo scale for UV and visible photochemistry. *Org Process Res Dev*. 2020;24:201-206.
33. Hubacz R, Wroński S. Horizontal Couette–Taylor flow in a two-phase gas–liquid system: flow patterns. *Exp Therm Fluid Sci*. 2004;28: 457-466.
34. Gao X, Kong B, Vigil RD. CFD investigation of bubble effects on Taylor–Couette flow patterns in the weakly turbulent vortex regime. *Chem Eng J*. 2015;270:508-518.
35. Ramezani M, Haghighat A, Legg MJ, Vigil RD, Olsen MG. Evolution of bubble size distribution, number density, and shape in semi-batch vertical gas–liquid Taylor vortex flow. *AIChE J*. 2020;66:e17003.
36. Gao X, Kong B, Ramezani M, Olsen MG, Vigil RD. An adaptive model for gas–liquid mass transfer in a Taylor vortex reactor. *Int J Heat Mass Transf*. 2015;91:433-445.
37. Ramezani M, Kong B, Gao X, Olsen MG, Vigil RD. Experimental measurement of oxygen mass transfer and bubble size distribution in an air–water multiphase Taylor–Couette vortex bioreactor. *Chem Eng J*. 2015;279:286-296.
38. Ramezani M, Legg MJ, Haghighat A, Li Z, Vigil RD, Olsen MG. Experimental investigation of the effect of ethyl alcohol surfactant on oxygen mass transfer and bubble size distribution in an air-water multiphase Taylor–Couette vortex bioreactor. *Chem Eng J*. 2017;319:288-296.
39. Dłuska E, Wroński S, Ryszczuk T. Interfacial area in gas–liquid Couette–Taylor flow reactor. *Exp Therm Fluid Sci*. 2004;28:467-472.
40. Dłuska E, Wroński S, Hubacz R. Mass transfer in gas–liquid Couette–Taylor flow reactor. *Chem Eng Sci*. 2001;56:1131-1136.
41. Noël T, Hessel V. Membrane microreactors: gas–liquid reactions made easy. *ChemSusChem*. 2013;6:405-407.
42. Hone CA, Kappe CO. Membrane microreactors for the on-demand generation, separation, and reaction of gases. *Chem A Eur J*. 2020;26: 13108-13117.
43. Gavriilidis A, Constantinou A, Hellgardt K, et al. Aerobic oxidations in flow: opportunities for the fine chemicals and pharmaceuticals industries. *React Chem Eng*. 2016;1:595-612.
44. Venezia B, Douthwaite M, Wu G, et al. Slurry loop tubular membrane reactor for the catalysed aerobic oxidation of benzyl alcohol. *Chem Eng J*. 2019;378:122250.
45. Wroński S, Dłuska E, Hubacz R, Molga E. Mass transfer in gas–liquid Couette–Taylor flow in membrane reactor. *Chem Eng Sci*. 1999;54: 2963-2967.
46. Fischel RJ, Fischel H, Shatzel A, Lance WPCD, Gervais D, Ascher NL. Couette membrane filtration with constant shear stress. *ASAIO Trans*. 1988;34:375-385.
47. Beaudoin G, Jaffrin MY. Plasma filtration in Couette flow membrane devices. *Artif Organs*. 1989;13:43-51.
48. Kaplan AA, Halley SE. Plasma exchange with a rotating filter. *Kidney Int*. 1990;38:160-166.
49. Lueptow RM, Hajiloo A. Flow in a rotating membrane plasma separator. *ASAIO J*. 1995;41:182-188.
50. Ohashi K, Tashiro K, Kushiya F, et al. Rotation-induced Taylor vortex enhances filtrate flux in plasma separation. *ASAIO Trans*. 1988;34: 300-307.
51. Lee S, Lueptow RM. Rotating reverse osmosis: a dynamic model for flux and rejection. *J Membr Sci*. 2001;192:129-143.
52. Lee S, Lueptow RM. Experimental verification of a model for rotating reverse osmosis. *Desalination*. 2002;146:353-359.
53. Lee S, Lueptow RM. Control of scale formation in reverse osmosis by membrane rotation. *Desalination*. 2003;155:131-139.
54. Shah TN, Yoon Y, Pederson CL, Lueptow RM. Rotating reverse osmosis and spiral wound reverse osmosis filtration: a comparison. *J Membr Sci*. 2006;285:353-361.
55. Hallström B, Lopez-Leiva M. Description of a rotating ultrafiltration module. *Desalination*. 1977;24:273-279.
56. Vigo F, Uliana C, Lupino P. The performance of a rotating module in oily emulsions ultrafiltration. *Sep Sci Technol*. 1985;20:213-230.
57. Min K, Lueptow RM. Circular Couette flow with pressure-driven axial flow and a porous inner cylinder. *Exp Fluids*. 1994;17:190-197.
58. Wereley ST, Akonur A, Lueptow RM. Particle–fluid velocities and fouling in rotating filtration of a suspension. *J Membr Sci*. 2002;209: 469-484.
59. Kroner KH, Nissinen V. Dynamic filtration of microbial suspensions using an axially rotating filter. *J Membr Sci*. 1988;36:85-100.
60. Schwille JA, Mitra D, Lueptow RM. Design parameters for rotating cylindrical filtration. *J Membr Sci*. 2002;204:53-65.
61. Holeschovsky UB, Cooney CL. Quantitative description of ultrafiltration in a rotating filtration device. *AIChE J*. 1991;37:1219-1226.
62. Greene JF, Preger Y, Stahl SS, Root TW. PTFE-membrane flow reactor for aerobic oxidation reactions and its application to alcohol oxidation. *Org Process Res Dev*. 2015;19:858-864.
63. Levenspiel O. *Chemical Reactor Engineering*. 3rd ed. John Wiley & Sons; 1999.
64. Richter O, Hoffmann H, Kraushaar-Czarnetzki B. Effect of the rotor shape on the mixing characteristics of a continuous flow Taylor-vortex reactor. *Chem Eng Sci*. 2008;63:3504-3513.
65. Rossi D, Gargiulo L, Valitov G, Gavriilidis A, Mazzei L. Experimental characterization of axial dispersion in coiled flow inverters. *Chem Eng Res Des*. 2017;120:159-170.
66. Nishimura T, Onoue T, Ohe K, Uemura S. Palladium(II)-catalyzed oxidation of alcohols to aldehydes and ketones by molecular oxygen. *J Org Chem*. 1999;64:6750-6755.
67. Steinhoff BA, Guzei IA, Stahl SS. Mechanistic characterization of aerobic alcohol oxidation catalyzed by $Pd(OAc)_2$/pyridine including identification of the catalyst resting state and the origin of nonlinear [catalyst] dependence. *J Am Chem Soc*. 2004;126:11268-11278.
68. Ye X, Johnson MD, Diao T, Yates MH, Stahl SS. Development of safe and scalable continuous-flow methods for palladium-catalyzed aerobic oxidation reactions. *Green Chem*. 2010;12:1180-1186.
69. Moore CMV, Cooney CL. Axial dispersion in Taylor–Couette flow. *AIChE J*. 1995;41:723-727.
70. Nemri M, Climent E, Charton S, Lanoë J-Y, Ode D. Experimental and numerical investigation on mixing and axial dispersion in Taylor–Couette flow patterns. *Chem Eng Res Des*. 2013;91:2346-2354.
71. Recktenwald A, Lücke M, Müller HW. Taylor vortex formation in axial through-flow: linear and weakly nonlinear analysis. *Phys Rev E*. 1993; 48:4444-4454.

72. Grossmann S, Lohse D, Sun C. High-Reynolds number Taylor–Couette turbulence. *Annu Rev Fluid Mech*. 2016;48:53-80.
73. Ostilla-Mónico R, van der Poel EP, Verzicco R, Grossmann S, Lohse D. Exploring the phase diagram of fully turbulent Taylor–Couette flow. *J Fluid Mech*. 2014;761:1-26.
74. Carey CS, Schlender AB, Andereck CD. Localized intermittent short-wavelength bursts in the high-radius ratio limit of the Taylor–Couette system. *Phys Rev E*. 2007;75:016303.
75. Benjamin TB, Mullin T. Anomalous modes in the Taylor experiment. *Proc R Soc A Math Phys Sci*. 1981;377:221-249.
76. Benjamin TB. Bifurcation phenomena in steady flows of a viscous fluid II. Experiments. *Proc R Soc A Math Phys Sci*. 1978;359:27-43.
77. Benjamin TB. Bifurcation phenomena in steady flows of a viscous fluid. I. Theory. *Proc R Soc A Math Phys Sci*. 1978;359:1-26.
78. Nakamura I, Toya Y, Yamashita S, Ueki Y. An experiment on a Taylor vortex flow in a gap with a small aspect ratio: bifurcation of flows in a symmetric system. *JSME Int J II Fluid*. 1990;33:685-691.
79. Nakamura I, Toya Y. Existence of extra vortex and twin vortex of anomalous mode in Taylor vortex flow with a small aspect ratio. *Acta Mech*. 1996;117:33-46.
80. Kataoka K, Doi H, Kongo T, Futagawa M. Ideal plug-flow properties of Taylor vortex flow. *J Chem Eng Jpn*. 1975;8:472-476.
81. Pudjiono PI, Tavare NS, Garside J, Nigam KDP. Residence time distribution from a continuous Couette flow device. *Chem Eng J*. 1992;48:101-110.
82. Yim SSS, Lo MYA, Titchener-Hooker N, Shamlou PA. The dependence of residence time distribution on flow in co-axial cylinder devices. *Bioprocess Eng*. 1998;19:221-227.
83. Enokida Y, Nakata K, Suzuki A. Axial turbulent diffusion in fluid between rotating coaxial cylinders. *AIChE J*. 1989;35:1211-1214.
84. Campero RJ, Vigil RD. Axial dispersion during low Reynolds number Taylor–Couette flow: intra-vortex mixing effects. *Chem Eng Sci*. 1997;52:3303-3310.
85. Nemri M, Charton S, Climent E. Mixing and axial dispersion in Taylor–Couette flows: the effect of the flow regime. *Chem Eng Sci*. 2016;139:109-124.
86. Lueptow RM, Docter A, Min K. Stability of axial flow in an annulus with a rotating inner cylinder. *Phys Fluids*. 1992;4:2446-2455.
87. Giordano RC, Giordano RLC, Prazeres DMF, Cooney CL. Analysis of a Taylor–Poiseuille vortex flow reactor—I: flow patterns and mass transfer characteristics. *Chem Eng Sci*. 1998;53:3635-3652.

SUPPORTING INFORMATION

Additional supporting information can be found online in the Supporting Information section at the end of this article.

How to cite this article: Venezia B, Morris DC, Gavriilidis A. Taylor-vortex membrane reactor for continuous gas–liquid reactions. *AIChE J*. 2022;e17880. doi:10.1002/aic.17880